Comparative Medicine
Copyright 2001
by the American Association for Laboratory Animal Science

Vol 51, No 2
April 2001
Pages 138-144

Three-dimensional Magnetic Resonance Imaging of Lung and Liver Tumors in Mice by Use of Transversal Multislice Magnetic Resonance Images

Taketoshi Asanuma, DVM, PhD[1], Kaori Ohkura, DVM[1], Tuyoshi Yamamoto, PhD[2], Yoshihiro Kon, DVM, PhD[3], Shigezou Shimokawa, PhD[4], and Mikinori Kuwabara, PhD[1,*]

Purpose: **To diagnose lung and liver tumors experimentally induced in mice in three-dimensional magnetic resonance (MR) images constructed by superimposing transversal multislice MR images of thoracic and abdominal regions taken under a high magnetic field of 7.05 tesla (T).**

Methods: **Lung and liver tumors were induced by administration of urethane to A/J mice and implantation of transplantable colon-26 cells into BALB/c mice, respectively. Two-dimensional (2-D) multislice MR images from the thoracic to abdominal regions were taken under the proton density-weighted conditions. Each organ in the 2-D MR images was pseudocolored, and a three-dimensional (3-D) image was constructed by superimposing them on a UNIX computer, using volume-rendering software.**

Results: **In the normal mouse, each organ in the thoracic and abdominal regions was three-dimensionally imaged and was clearly distinguished from the others. In mice with tumors in the lung or liver, the pathologic changes in the tissue could be visualized in 3-D images.**

Conclusions: **The MR images three-dimensionally constructed by use of a method combining MR imaging under a high magnetic field of 7.05 T and a computer technique using volume-rendering software was useful for diagnosis of lung and liver tumors experimentally induced in mice.**

Magnetic resonance imaging (MRI) is a noninvasive, nondestructive tool used for clinical diagnosis in human and veterinary medicine. For its application to small laboratory animals, such as mice and rats, we tried to visualize pathologic changes in their tissues and reported the successful results for hepatocellular carcinoma in Long-Evans Cinnamon (LEC) rats and age-dependent morphologic changes in brains of Wistar rats by use of an MRI apparatus equipped with a magnet producing a high magnetic field of 7.05 tesla (T) (1-4). We also reported that visualization of the topographic structure of the mouse brain was achieved by a use of a method combining a strong gradient coil and a magnet producing a high, extremely uniform magnetic field (5). However, there was a limit to understanding the precise anatomy of the lesions and their related structures from two-dimensionally projected images.

Recently, methods such as computed tomography (CT) angiography, MRI and MR-angiography containing three-dimensional (3-D) volume data have been developed to obtain much information about anatomic structures (6-16). The reconstructed 3-D images helped to comprehend the precise anatomy of lesions and their related structures. The volume-rendering software used was a program that displays 3-D constructed images (13, 15, 17, 18). The 3-D image constructed by this program includes information about not only the surface of the tissue, but also its interior structure, and the 3-D image obtained from this program provides more data than does surface rendering. This program has an additional function to accentuate foci and lesions after treating normal regions in the 3-D image so that they become transparent (18). In the study reported here, we applied this MRI method to three-dimensionally visualize the cranial portion of the abdomen and thorax of the mouse to diagnose disease models.

For this purpose, we experimentally induced tumors in the lung and liver in mice by administrating urethane and transplanting colon-26 cells, respectively, then detecting them in 3-D images constructed by use of this volume-rendering program. The lung tumors were induced by intraperitoneal (i.p.) injection of a chemical carcinogen, urethane, into the A/J mouse (19, 20). The liver tumors were created by intraportal implantation of mouse transplantable colon-26 cells, which is regarded as an experimental model of liver metastasis of colorectal cancer (21, 22). Before MR imaging, we administered a positive-contrast agent, Ferri Seltz, to the gastrointestinal tract to distinguish it from the surrounding tissues (liver, spleen, kidney, heart, bone, and spine) (23-25).

Materials and Methods

Mice. Specific-pathogen-free male A/J mice (8 weeks old, n = 6) and BALB/c mice (8 weeks old, n = 6) were obtained from Japan SLC, Inc. (Hamamatsu, Japan). All mice were maintained under conventional conditions and were cared for humanely according to the guidelines set by the Hokkaido University Veterinary Medicine Animal Care and Use Committee. They were fed a regular diet and water ad libitum in an air-conditional animal room at 22 ±3°C, with relative humidity of 55 ±5% (1-3).

[1]Laboratory of Radiation Biology and [3]Laboratory of Experimental Animal Science, Graduate School of Veterinary Medicine, Hokkaido University, Sapporo 060-0818, [2]Division of Electronics and Information Engineering, Graduate School of Engineering, Hokkaido University, Sapporo 060-0818, and [4]Technoscience Laboratory Company, Ltd., Ebetsu 069-0854, Japan.
**Corresponding author.*

Tumor induction in lung. The A/J strain of mice was used as the model for lung tumors induced by urethane. According to the method of Malkinson (22), 1 g of urethane/kg of body weight dissolved in 0.9% NaCl was administered i.p. into 8-week-old mice (n = 6). Lung tumors appeared at 10 to 12 weeks after injection. Twenty-four weeks after injection, the images of the thoracic cavity of mice were initially obtained from living mice, but the movement of breathing and the heart beat interfered with detection of the small tumor. Then mice were sacrificed by subcutaneous administration of an overdose of rapid injection of pentobarbital sodium solution (200 mg/kg, Dainippon Pharmaceutical Co., Osaka, Japan) to avoid the effects of respiratory motion on MR images of the thorax after administrating a positive-contrast agent into the stomach and duodenal cavities.

Tumor induction in liver. The BALB/c strain of mice was used as the pathologic model for liver tumors induced by implantation of colon-26 cells, which were kindly provided by Dr. Y. Sato, First Department of Surgery, Hokkaido University School of Medicine. Cells were cultured in RPMI 1640 medium supplemented with 10% fetal bovine serum. Mice were anesthetized with diethyl ether then were laparotomized, and 0.1 ml of colon-26 suspension including 10^4 cells was administered into the thoracic mesenteric vein. The liver tumors appeared at 10 days after implantation. Fourteen days after implantation, mice were anesthetized with a pentobarbital sodium solution (40 mg/kg) diluted 2.5 times with a mixed solution of propylene glycol/ethanol/H_2O (2/1/7, wt/wt) for MR imaging after administrating a positive-contrast agent into the stomach and duodenal cavities.

Magnetic resonance imaging. A positive-contrast agent, Ferri Seltz (Ohtsuka Pharmaceutical Co., Tokushima, Japan), at a dosage of 70 mg/kg was orally administrated into the stomach and duodenal cavities through a catheter just before imaging. For MR imaging of liver tumors, a parasympathetic blocker, scopolamine butylbromide (Tanabe Pharmaceutical Co., Osaka, Japan), was injected i.p. into mice to prevent motional artifacts in MR images due to peristalsis. An imaging probe (a low inductance saddle-shaped coil) for mice designed in similar manner as that described (1, 2) was used. A Teflon sheet with adequate thickness was inserted between two layers of copper film as an insulator to make the probe resonate at 300 MHz. Proton MR images at 7.05 T were obtained as described (1-5). After sacrifice (lung tumor model) or anesthetization (liver tumor model), each mouse was positioned supine in the probe running parallel to the z-axis of the magnet. In the case of anesthetized mice, they were further fixed to a cradle, using adhesive tape to minimize the artifacts due to respiratory motions. An acrylic tube (5 mm in diameter, 10 mm long) containing mineral oil was set under the mouse and was used as a standard for the image intensity. Sagittal scout images of the body were first obtained under T1-weighted conditions (TR/TE= 500/20 ms) to determine the positions of transversal sections. Proton density-weighted MR images (TR/TE=2,000/20 ms) were then taken, using multislice spin-echo sequence with four acquisitions. The following parameters were also used: field of view (FOV), 3×3 cm^2; slice thickness, 1.0 mm; data matrix size, 256×256; pixel matrix size for reconstructed images, 512×512.

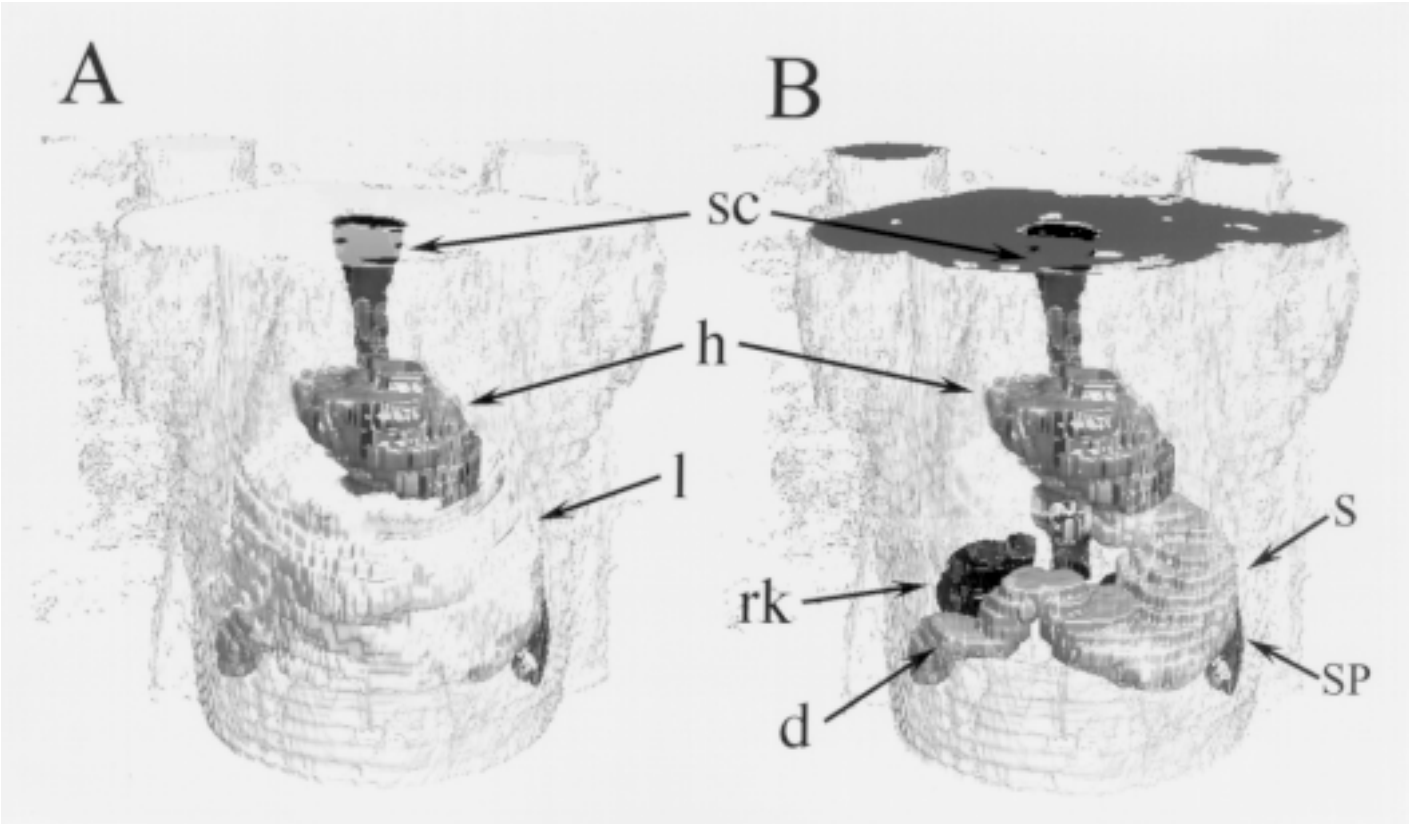

Figure 1. Three-dimensional magnetic resonance (MR) images of a normal mouse from the thorax to the upper abdominal region, (A) constructed by changing the opacity of non-colored regions to 15% (sc = spinal cord, h = heart, l = liver), and (B) constructed by changing the opacities of non-colored regions to 15% and those of the liver and gallbladder to 0%. (s = stomach, rk = right kidney, sp = spleen, d = duodenum).

Construction of 3-D images. To distinguish several organs (heart, liver, gallbladder, stomach, duodenum, kidney, spinal cord, and tumor) from each other, each organ on the multislice MR image was pseudocolored, using a Power MacIntosh model 7600/132 (Apple Computer. Inc., Cupertino, Calif.) with the imaging program Photshop (Adobe Systems, San Jose, Calif.). After pseudocolorization, 3-D construction was performed, using a UNIX workstation with a personally made volume-rendering program (volume ray tracing) (18). Additionally, this program could make a 3-D image of a particular region or organ translucent by changing its opacity from 100% to 0%. Furthermore, it could turn the 3-D image around the z-axis and x- or y-axis in an arbitrary degree arc.

Histologic examination. After MR imaging followed by euthanasia by administration of an anesthetic overdose, lung and liver tissues were removed and fixed with neutral-buffered 10% formalin, then were embedded in paraffin wax and sectioned at 5-μm thickness. Each section was stained with hematoxylin and eosin and examined microscopically to evaluate the lesions.

Results

Three-dimensional MR images of thoracic and abdominal regions in normal mice. Three-dimensional MR images from thoracic to abdominal regions in normal mice are shown in Fig. 1 (A and B). The two dorsal pillars are the phantom used as a standard. The heart, liver, gallbladder, stomach, duodenum, kidney, and spinal cord were pseudocolored on each 2-D multislice MR image taken under proton density-weighted conditions, then the 3-D image was constructed under conditions in which the opacity of the non-colored (gray-colored) regions of the original MR image was 15%. Though the figures are shown as monochromatic images, the heart (h), liver (l) and spinal cord (sc) were distinguished from each other with respect to their position, size, and shape by use of this method. However, it was found that

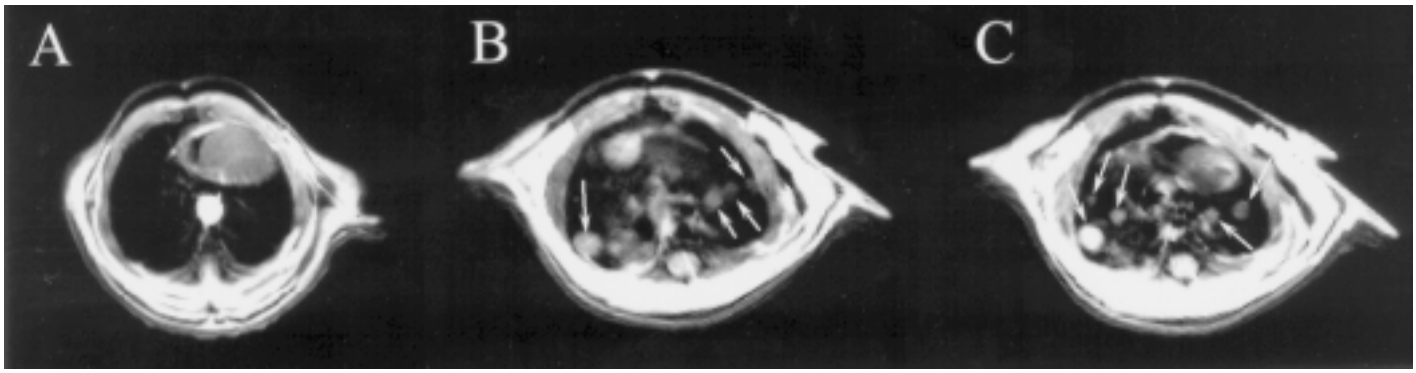

Figure 2. The MR images of thoracic regions of (A) a normal mouse and (B) a urethane-treated mouse. (C) The MR image of the thoracic regions of a urethane-treated, euthanized mouse. Arrows indicate tumors in the lung.

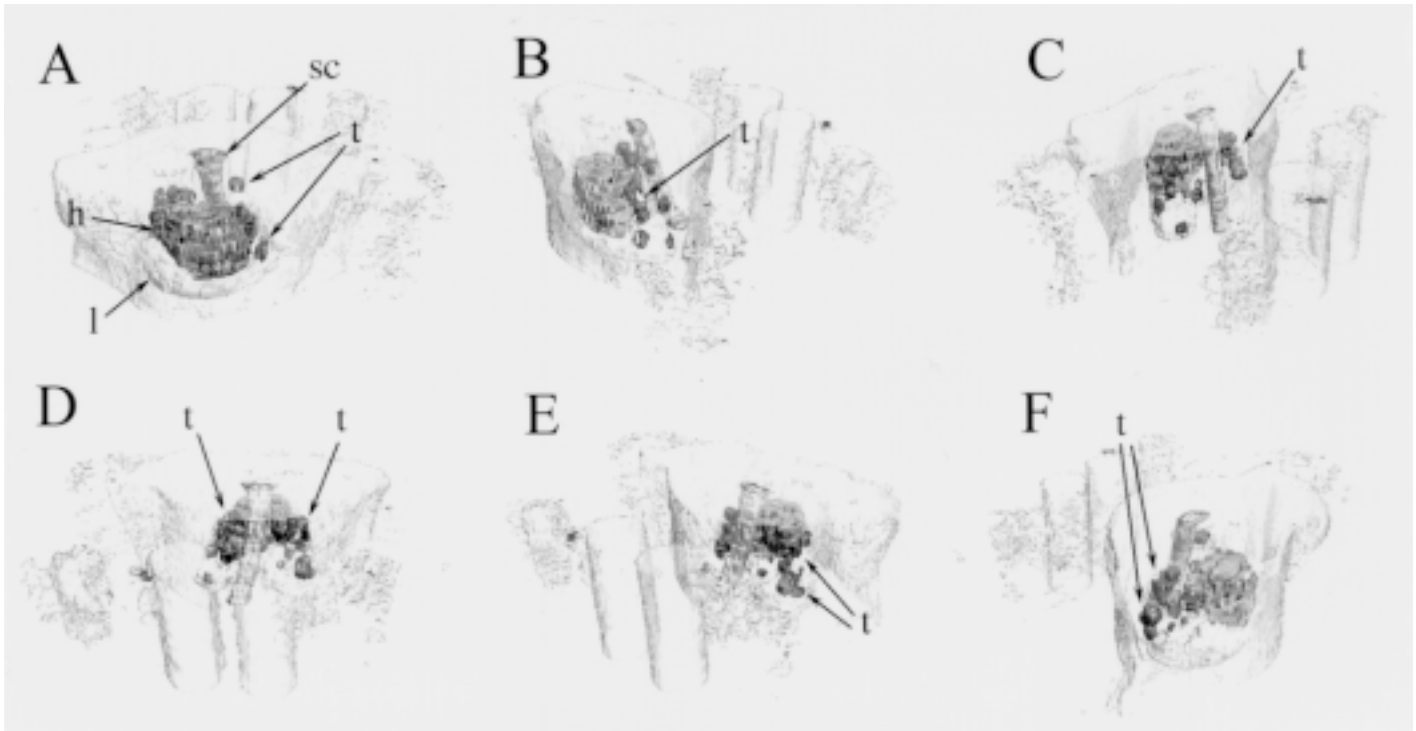

Figure 3. Three-dimensionally reconstructed MR images (A to F) of the thoracic region of a urethane-treated mouse seen from the directions 0, 60, 120, 180, 240, and 300 degrees around the z-axis, respectively (t = tumor). *See* Figure 1 for key.

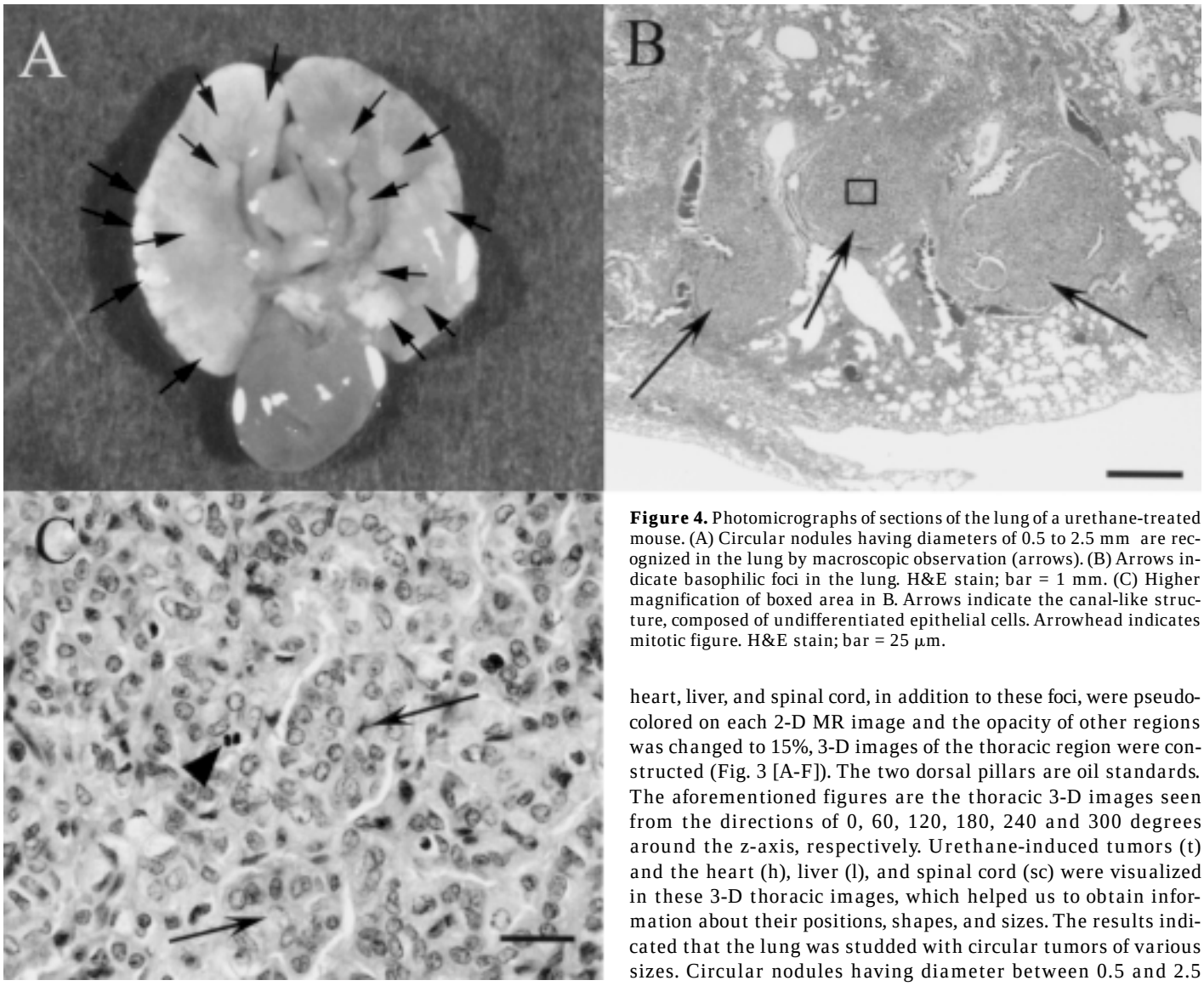

Figure 4. Photomicrographs of sections of the lung of a urethane-treated mouse. (A) Circular nodules having diameters of 0.5 to 2.5 mm are recognized in the lung by macroscopic observation (arrows). (B) Arrows indicate basophilic foci in the lung. H&E stain; bar = 1 mm. (C) Higher magnification of boxed area in B. Arrows indicate the canal-like structure, composed of undifferentiated epithelial cells. Arrowhead indicates mitotic figure. H&E stain; bar = 25 μm.

the region corresponding to the liver largely covered other regions (Fig. 1A). When the opacity of the liver and gallbladder was changed to 0%, the stomach (s), duodenum (d), right kidney (rk), and spleen (sp) could be visualized as shown in Fig. 1B. Though these images could be rotated around the x-axis or its horizontal directions, only the image seen from the ventral direction was demonstrated.

Three-dimensional MR images of urethane-induced lung tumors. Fig. 2A shows a proton-density-weighted thoracic MR image of a normal mouse. The lung was imaged as dark regions because of its low proton density. However, several regions with strong MR signal intensities, which might be assigned to lung tumors, appeared in urethane-treated mice (Fig. 2B). The lung was studded with circular lesions, large and small, strong and weak, as indicated by arrows. Fig. 2C is a 2-D thoracic image of a sacrificed mouse that could be more sharply obtained than that of an anesthetized mouse as shown in Fig. 2B. Small foci could be further detected in this image. Therefore, transversal MR images of sacrificed mice were used to construct accurate 3-D MR images of tumors in the thoracic regions. After the heart, liver, and spinal cord, in addition to these foci, were pseudocolored on each 2-D MR image and the opacity of other regions was changed to 15%, 3-D images of the thoracic region were constructed (Fig. 3 [A-F]). The two dorsal pillars are oil standards. The aforementioned figures are the thoracic 3-D images seen from the directions of 0, 60, 120, 180, 240 and 300 degrees around the z-axis, respectively. Urethane-induced tumors (t) and the heart (h), liver (l), and spinal cord (sc) were visualized in these 3-D thoracic images, which helped us to obtain information about their positions, shapes, and sizes. The results indicated that the lung was studded with circular tumors of various sizes. Circular nodules having diameter between 0.5 and 2.5 mm, with an average number of 30 (n = 6), were recognized in the lung by macroscopic observation (arrows in Fig. 4A). The basophilic foci were diagnostic of adenocarcinoma characterized by well demarcated, non-encapsulated nodules of neoplastic epithelial nests and minimal intervening stroma by use of microscopic observation (Figs. 4B and 4C). Under the proton-density weighting, signal intensity of foci might reflect the stage of carcinoma (Figs. 2B and 2C).

Three-dimensional MR images of colon 26-induced liver tumors. Fig. 5 (A-C) are MR images of the liver of a mouse in which colon-26 cells were implanted. The MR images were obtained under proton density-weighted (TR/TE = 2,000/20 ms, Fig. 5A), T1-weighted (TR/TE = 500/20 ms, Fig. 5B) and T2-weighted conditions (TR/TE = 2,000/80 ms, Fig. 5C). A proton density-weighted MR image of the liver of a normal mouse is shown in Fig. 5D. Asterisks represent the stomach region enhanced by use of the positive-contrast agent. Abnormal hyperintense regions were observed in the liver under all conditions, as indicated by arrows (Figs. 5A-5C). These regions were especially clearly visualized under the T2-weighting (Fig. 5C), and might be assigned to colon 26-induced tumors. Since the signal inten-

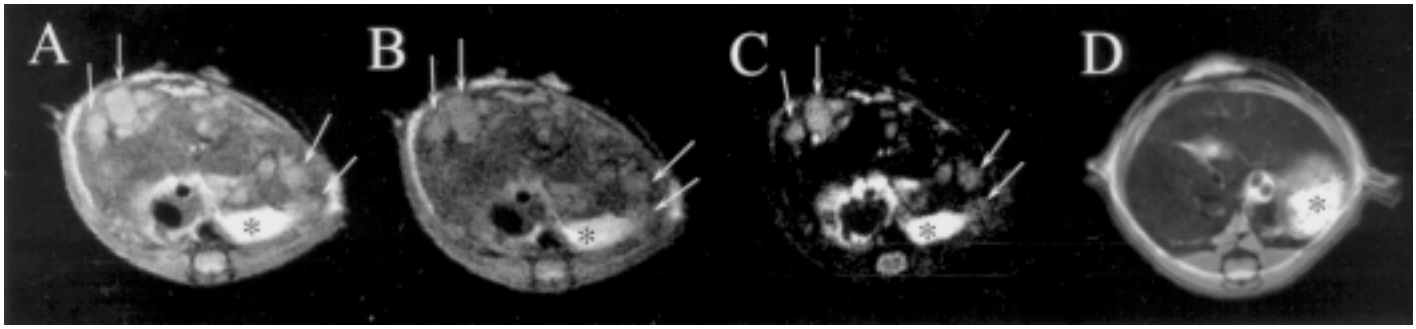

Figure 5. Two-dimensional MR images of the liver of a colon 26-implanted mouse: (A) proton density-weighted (TR/TE = 2,000/20 ms), (B) T1-weighted (TR/TE = 500/20 ms), and (C) T2-weighted (TR/TE = 2,000/80 ms). (D) Two-dimensional MR image of the liver of a normal mouse taken under the proton-density-weighted condition. Asterisks indicate stomach enhanced by the positive-contrast agent Ferri Seltz. Arrows indicate pathologic alterations originating from implantation of colon-26 cells.

sities of regions other than these hyperintense ones seemed to increase in colon 26-implanted mice under proton- density imaging if the MR image in Fig. 5A was compared with that in Fig. 5D, tumors that were undetectable by MRI might have diffused into the whole liver. After the hyperintense regions in Fig. 5A were pseudocolored to distinguish them from normal regions in each 2-D image, a 3-D image of the liver with tumors was constructed (Figs. 6A and 6B). The two dorsal pillars show the phantom as a standard. Figs. 6A and 6B show MR images of the abdominal region of a colon 26-implanted mouse before and after the opacity of normal regions in the liver was changed to 0% (l), respectively. In Fig. 6A, tumor regions were largely covered by the whole liver (designated l), but in the translucent image at the normal regions of liver (Fig. 6B), these were clearly visualized with respect to their position and shape (designated t). The tumors appeared to lie sporadically around liver veins, suggesting that the colon-26 cells spread over a considerable region of the liver and grew. In addition, the boundaries of individual lesions seemed to be obscure.

Variously sized and shaped foci were observed on the surface of the liver by macroscopic observation (data not shown). Metastatic nodules were not observed in other organs. Histologic results obtained by microscopic observations are shown in Fig. 7 (A and B). Basophilic small nodules indicated by arrows were detected in the liver (Fig. 7A). These nodules were mainly composed of undifferentiated cells, in which many mitotic figures were observed. These regions contained various shapes, circular and elliptical, but a bile duct-like structure was not detected in tumors throughout the liver (Fig. 7B). Therefore, these nodules were identified as undifferentiated carcinoma, which was observable by MRI under the proton density-weighted and T2-weighted conditions (Figs. 5A and 5C).

Discussion

Diagnosis of pathologic changes in tissues and organs by use of 3-D imaging techniques has progressed remarkably and is widely used for humans and animals (7, 11, 15, 16). Spiral CT in particular enables simultaneous display of 3-D images of the breast cavity (11). Hahn and co-workers (26) reported the application of 3-D MRI to small laboratory animals. In the study reported here, the construction of 3-D images, using transversal multislice MR images of thoracic and abdominal regions of mice taken under a high magnetic field of 7.05 T, was carried out to diagnose experimentally induced lung and liver tumors. To distinguish the gastrointestinal tract from the surrounding tissues, we administered a positive-contrast agent, Ferri Seltz, to it. Then, two-dimensional transversal multislice MR images of thoracic and abdominal regions were taken under a high magnetic field of 7.05 T in proton density-weighted conditions. After the organs in the thoracic and abdominal regions were pseudocolored, the construction of 3-D MR images was carried out by superimposing them, using a UNIX workstation and a personally made volume-rendering program (18). Thus, individual organs were clearly distinguished from other organs with respect to their position, size, and shape in pseudocolored 3-D images. These organs are shown as monochromatic images in Fig. 1 (A and B).

In urethane-treated and colon 26-implanted mice, the pathologic changes in tissues were recognized by use of this 3-D MR imaging technique. Complete information about the position, shape, and size or urethane-induced lung tumors was obtained from 3-D images seen from various directions (Figs. 3A-3F). This is an advantageous aspect of the 3-D MR imaging method used in this study. Magnetic resonance imaging shows tumors with various signal intensities depending on the type, growth rate, and water content (27). Figs. 2B and 2C are MR images of lungs of living and euthanized mice, respectively. Urethane-induced tumors were detectible in both groups, suggesting that there was not excess water in the normal lung even in the euthanized mice.

Colon 26-induced tumors in the liver with obscure boundaries were visualized in 3-D images though individual ones were distinguished from each other in 2-D images under proton density-weighting. Because the tumors were close together in the liver, it was hard to construct 3-D images showing them separately. Colon 26-induced tumors were present at the edge of the liver and were located apart from its center. This might indicate that colon-26 cells were carried to the inside of the liver by the cranial mesenteric vein and grew there. Colon 26-induced tumors were visualized as hyperintense regions under T1-weighting in 2-D MR images. This was in contrast to the general observation that tumors were visualized as hypointense regions under T1-weighting, because T1 relaxation times of tumors usually tend to become longer than those of normal tissues (27). It will be necessary to measure the exact T1 and T2 relaxation times of tumor-bearing livers and normal ones under the high magnetic field of 7.05 T to explain this controversial observation.

A positive-contrast agent was used in this study. This agent made of paramagnetic ions significantly shortened the T1 and T2 relaxation times. The relaxation times of water protons correlate strongly to the iron concentration in tissue (23-26, 28). Koga and co-workers (24) reported that a high-contrast image

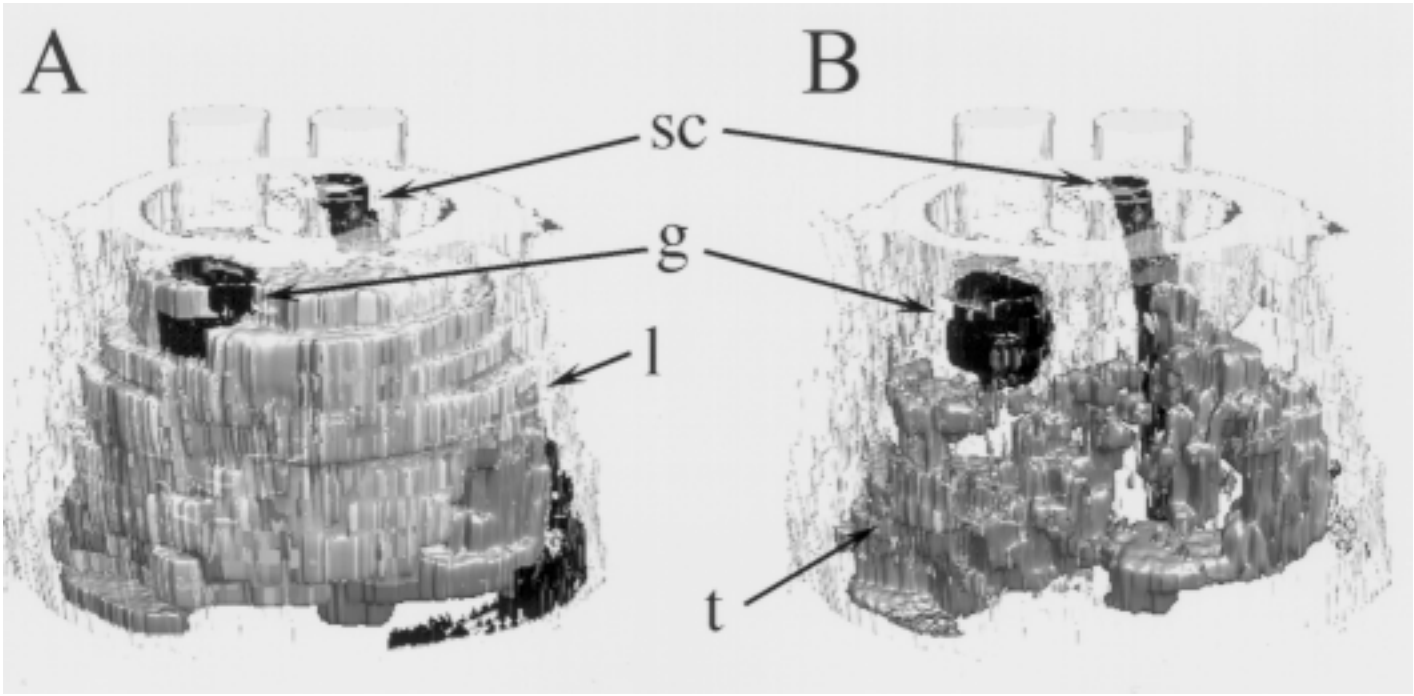

Figure 6. Three-dimensional MR images of colon 26-induced tumors in the mouse liver, (A) constructed by changing the opacity of non-colored regions to 15% (g = gallbladder), (B) constructed by changing the opacities of non-colored regions to 15% and those of the liver to 0%, respectively. *See* Figure 3 for key.

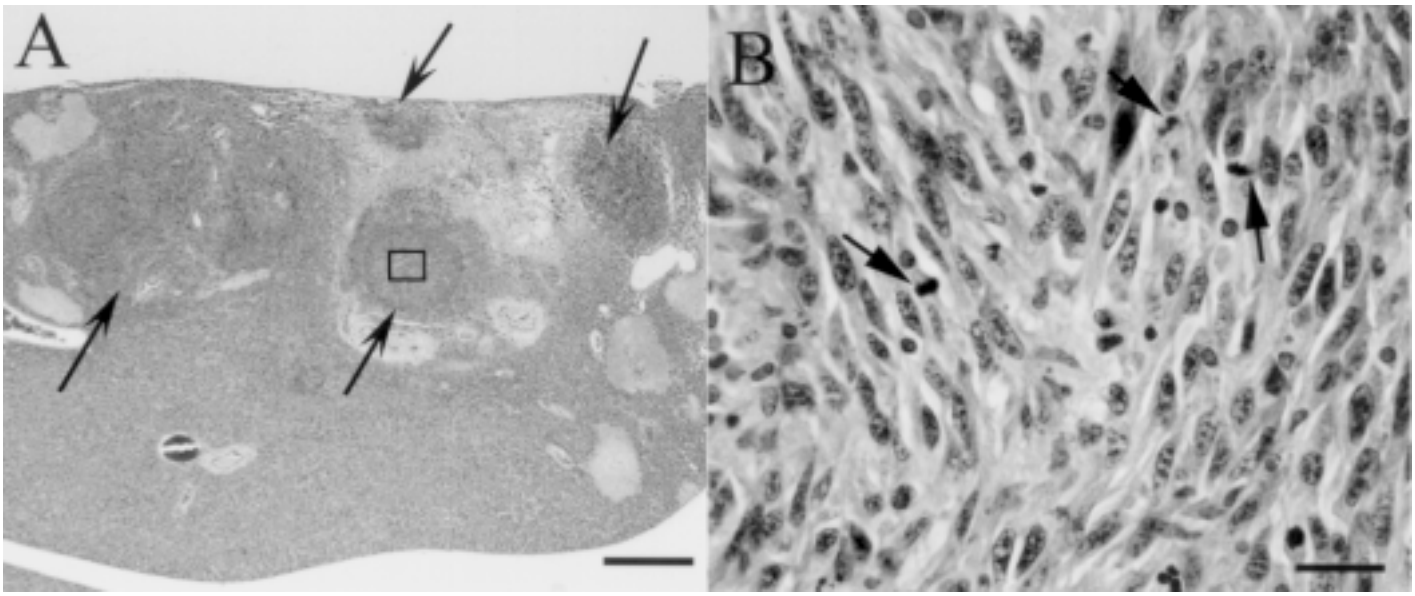

Figure 7. Histologic examination of colon 26-induced tumors in the mouse liver. (A) Arrows indicate basophilic small nodules of various shapes. H&E stain; bar = 1 mm. (B) Higher magnification of boxed area in A. Arrows indicate mitotic figures. A bile duct-like structure is not detected in tumors. H&E stain; bar = 25 μm.

under T1-weighting (TR/TE = 500/20 ms) with a magnetic field of 4.7 T was detectable in rats in which the stomach was filled with the contrast agent. In our preliminary experiment, T1 and T2 relaxation times of distilled water were found to be around 3,000 milliseconds, whereas those from use of the Ferri Seltz solution at a concentration of 10 g/L were 340 ± 20, 280 ± 35 milliseconds, respectively, were significantly shorter than those of pure water. Since the relaxation times were shortened at 7.05 T, this contrast agent was expected to be useful for MR imaging of small laboratory animals. Actually, this positive-contrast agent was useful to distinguish the stomach, duodenum, and other abdominal organs of the mouse.

The reconstructed 3-D images had jagged and discontinuous structures, especially as shown in Fig. 6. A slice thickness of 1 to 1.5 mm is sufficiently thin for the construction of 3-D images of the human body, but is large for the mouse body (15). Our program consisting of a volume-ray tracing method constructs 3-D images with voxels corresponding to slice thickness (18). One-millimeter slices were too thick to construct a smooth 3-D image of the mouse body.

In this study, we tried to make MR images of normal, urethane-induced lung tumors and colon 26-induced liver tumors in mice, and reconstructed 3-D images using a personally made volume-rendering computer program. The results suggested that this 3-D technique for small laboratory animals might be widely applicable for diagnosis of pathologic changes in various tissues and organs.

Acknowledgments

We thank Y. Sato, First Department of Surgery, Hokkaido University School of Medicine, for kindly supplying mouse transplantable colon-26 cells as well as technically supporting us, C. Itakura, Laboratory of Comparative Pathology, Graduate School of Veterinary Medicine, for helpful discussion, and Mr. E. Yamada, Laboratory of Nuclear Magnetic Resonance, Faculty of Engineering, for technical assistance. This research was supported in part by a Grant-in-Aid for Basic Scientific Research from the Ministry of Education, Science, Sports and Culture of Japan (No. 09556064 to M. K.). In conducting this work, the investigators adhered to *The Guide for the Care and Use of Laboratory Animals*, Graduate School of Veterinary Medicine.

References

1. **Kuwabara, M., T. Asanuma, O. Inanami, T. Jin, S. Shimokawa, N. Kasai, K. Kator and F. Sato.** 1994. Magnetic resonance imaging of young and aged rat brains under a magnetic field of 7.05 T. J. Vet. Med. Sci. **55:**933-938.
2. **Inanami, O., T. Asanuma, N. Inukai, T. Jin, S. Shimokawa, N. Kasai, M. Nakano, F. Sato and M. Kuwabara.** 1995. The suppression of aged-related accumulation of lipid peroxides in rat brain by administration of Rooibos tea (*Aspalathus linearis*). Neurosci. Lett. **196:**85-88.
3. **Asanuma, T., Y. Hirano, K. Ohkura, Y. Kon, S. Shimokwa, N. Kasai and M. Kuwabara.** 1997. Magnetic resonance imaging of hepatocellular carcinoma in Long-Evans Cinnamon rats under a magnetic field of 7.05 T. Jpn. J. Vet. Res. **45:**147-151.
4. **Asanuma, T., Y. Hirano, K. Yamamoto, Y. Kon, S. Shimokawa and M. Kuwabara.** 1999. MR imaging of hepatic injury in the LEC rat under a high magnetic field (7.05 T). J. Vet. Med. Sci. **61:**239-244.
5. **Asanuma, T., S. Shimokawa, O. Inanami, Y. Kon and M. Kuwabara.** 1998. Visualization of the topographical structure of the anesthetized mouse brain by MR microimaging. J. Vet. Med. Sci. **60:**1311-1314.
6. **Axel, L., G. T. Herman, J. K. Udupa, P. A. Bottomley and W. A. Edelstein.** 1983. Three-dimensional display of nuclear magnetic resonance (NMR) cardiovascular images. J. Comput. Assist. Tomogr. **7:**172-174.
7. **Cullip, T. J., J. R. Symon, J. G. Rosenman, and E. L. Chaney.** 1993. Digitally reconstructed fluoroscopy and other interactive volume visualizations in 3-D treatment planning. Int. J. Radiat. Oncol. Biol. Phys. **27:**145-151.
8. **Cutting, C., F. L. Bookstein, B. Grayson, L. Fellingham and J. G. McGarthy.** 1986. Three-dimensional computer-assisted design of craniofacial surgical procedures: cephalometric and CT-based models. Plastic. Reconst. Surgery **77:**877-885.
9. **Fishman, E. K., B. Drebin, D. Magid, W. W. Scott Jr., D. R. Ney, A. F. Brooker Jr., L. H. Riley Jr., J. A. St. Ville, E. A. Zerhouni and S. S. Siegelman.** 1987. Volumetic rendering techniques: applications for three-dimensional imaging of the hip. Radiology **163:**737-738.
10. **Herman, G. T.** 1988. Three-dimensional imaging on a CT or MR scanner. J. Comput. Assist. Tomogr. **12:**450-458.
11. **Johnson, P. T., D. G. Heath, B. S. Kuszyk, and E. K. Fishman.** 1997. CT angiography: thoracic vascular imaging with interactive volume rendering technique. J. Compt. Assist. Tomogr. **21:**110-114.
12. **Lang, P., P. Steiger, H. K. Genant, N. Chafetz, T. Lindquist, S. Skinner and S. Moore.** 1988. Three-dimensional CT and MR imaging in congenital dislocation of the hip: clinical and technical considerations. J. Compt. Assist. Tomogr. **12:**459-464.
13. **Levin, D. N., X. Hu, K. K. Tan, and S. Galhotra.** 1989. Surface of the brain: three-dimensional MR images created with volume rendering. Radiology **171:**277-280.
14. **Levoy, M.** 1988. Display of surface from volume data. IEEE Comput. Graph. Appl. **8:**29-37.
15. **Nakajima, S., H. Atsumi, A. H. Bhalerao, F. A. Jolesz, R. Kikinis, T. Yohimine, T. M. Moriarty and P. E. Stieg.** 1997. Computer-assisted surgical planning for cerebrovascular neurosurgery. Neurosurgery **41:**403-410.
16. **Vannier, M. W., and J. L. Marsh.** 1996. Three-dimensional imaging, surgical planning, and imge-guided therapy. Radiol. Clin. North Am. **34:**545-563.
17. **Rusinek, H., M. R. Mourino, H. Firooznia, J. C. Weinreb and N. E. Chase.** 1989. Volume rendering of MR images. Radiology **171:**269-272.
18. **Yamamoto, T.** 1994. Visualization of time varying volume data. Bull. Fac. Eng. Hokkaido Univ. **167:**181-200 (in Japanese).
19. **Nettleship, A., P. S. Henshaw and H. L. Meyer.** 1943. Induction of pulmonary tumors in mice with ethyl carbamate (urethane). J. Nat. Cancer. Inst. **4:**309-320.
20. **Malkinson, A. M., M. N. Nesbitt, and E. Skamene.** 1985. Susceptibility to urethane-induced pulmonary adenomas between A/J and C57BL/6J mice: use of AXB and BXA recombinant inbred lines indicating a three-locus genetic model. J. Nat. Cancer Inst. **75:**971-974.
21. **Corbett, T. H., D. P. Griswold Jr., B. J. Roberts, J. C. Peckham and F. M. Schabel.** 1975. Tumor induction relationships in development of transplantable cancers of the colon in mice for chemotherapy assays, with a note on carcinogen structure. Cancer Res. **35:**2434-2439.
22. **Tominaga, T., Y. Yoshida, M. Kitamura, and G. Kosaki.** 1987. Liver metastasis of colon 26 cells implanted into the superior mesenteric vein in mice. Jpn. J. Cancer Res. (Gann) **78:**846-850.
23. **Hirohashi, S., H. Uchida, K. Yoshikawa, N. Fujita, K. Ohotomo, Y. Yuasa, Y. Kawamura and O. Matsui.** 1994. Large scale clinical evaluation of bowel contrast agent containing ferric ammonium citrate in MRI. Magn. Reson. Imaging **12:**837-846.
24. **Koga, K., J. Nakamura, T. Nakamura, and I. Miura.** 1990. MRI contrast enhancement of a new oral abdominal contrast agent containing ferric ammonium citrate. Jpn. J. Magn. Reson. Med. **10:**114-120 (in Japanese).
25. **Takahara, T., T. Yoshikawa, M. Saeki, S. Nosaka, K. Snimoyamada, Y. Nakajima and T. Ishikawa.** 1995. High concentration ferric ammonium citrate (FAC) solution as a negative bowel contrast agent. Nippon Acta Radiolo. **55:**425-426 (in Japanese).
26. **Hahn, P. F., D. D. Stark, S. Saini, J. M. Lewis, J. Wittenberg and J. T. Ferrucci.** 1987. Ferrite particles for bowel contrast in MR imaging: design issues and feasibility studies. Radiology **164:**37-41.
27. **Gadian, D. G.** 1995. NMR and its applications to living systems. Oxford University Press, Inc., New York.
28. **Saini, S., D. D. Stark, P. F. Hahn, J.-C. Bousquet, J. Introcasso, J. Wittenberg, T. J. Brady and J. T. Ferrucci Jr.** 1987. Ferrite particles: a superparamagnetic MR contrast agent for enhanced detection of liver carcinoma. Radiology **162:**217-222.